arXiv:1609.07490v1 [hep-ph] 23 Sep 2016

LAPTH-041/16

Monojet searches for momentum-dependent dark matter interactions

Daniele Barducci[a] , **Aoife Bharucha**[b] , **Nishita Desai**[c] , **Michele Frigerio**[d] , **Benjamin Fuks**[e,f] , **Andreas Goudelis**[e,f,g] , **Suchita Kulkarni**[g] , **Giacomo Polesello**[h] and **Dipan Sengupta**[i]

[a] *LAPTh, Université Savoie Mont Blanc, CNRS, B.P. 110, F-74941 Annecy-le-Vieux, France*

[b] *CNRS, Aix Marseille U., U. de Toulon, CPT, Marseille, France*

[c] *Institut für Theoretische Physik, Universität Heidelberg, Germany*

[d] *Laboratoire Charles Coulomb (L2C), UMR 5221 CNRS-Université de Montpellier, F-34095 Montpellier, France*

[e] *Sorbonne Universités, UPMC Univ. Paris 06, UMR 7589, LPTHE, F-75005 Paris, France*

[f] *CNRS, UMR 7589, LPTHE, F-75005 Paris, France*

[g] *Institute of High Energy Physics, Austrian Academy of Sciences, Nikolsdorfergasse 18, 1050 Vienna, Austria*

[h] *INFN, Sezione di Pavia, via Bassi 6, 27100 Pavia, Italy*

[i] *Laboratoire de Physique Subatomique et de Cosmologie, Université Grenoble-Alpes, CNRS/IN2P3, 53 Avenue des Martyrs, F-38026 Grenoble, France*

E-mail: daniele.barducci@lapth.cnrs.fr, aoife.bharucha@cpt.univ-mrs.fr, n.desai@thphys.uni-heidelberg.de, michele.frigerio@umontpellier.fr, fuks@lpthe.jussieu.fr, andreas.goudelis@lpthe.jussieu.fr, Suchita.Kulkarni@oeaw.ac.at, giacomo.polesello@cern.ch, dipan@lpsc.in2p3.fr

Abstract: We consider minimal dark matter scenarios featuring momentum-dependent couplings of the dark sector to the Standard Model. We derive constraints from existing LHC searches in the monojet channel, estimate the future LHC sensitivity for an integrated luminosity of 300 fb^{-1}, and compare with models exhibiting conventional momentum-independent interactions with the dark sector. In addition to being well motivated by (composite) pseudo-Goldstone dark matter scenarios, momentum-dependent couplings are interesting as they weaken direct detection constraints. For a specific dark matter mass, the LHC turns out to be sensitive to smaller signal cross-sections in the momentum-dependent case, by virtue of the harder jet transverse-momentum distribution.

Contents

1 Introduction **1**

2 Theoretical framework and constraints **3**
- 2.1 The minimal scenario: the Higgs portal 3
- 2.2 A pragmatic scenario with a scalar singlet mediator 4
- 2.3 Constraints on the parameters of the model 5

3 Numerical results **8**
- 3.1 Analysis setup 8
- 3.2 Bounds derived from LHC monojet data 10
- 3.3 Complementarity of collider, cosmological and theoretical considerations 12

4 Conclusion **15**

5 Acknowledgements **16**

A Derivation of perturbative unitarity constraints **16**

1 Introduction

Collider searches for final states consisting of a hard jet and missing energy [1–5], dubbed monojet searches, provide a means to detect new invisible particles that are stable on detector or even cosmological scales. In the latter case, these particles could contribute to the dark matter (DM) energy density of the Universe and monojet searches could offer invaluable information about their existence. Furthermore it is well known that the jet transverse-momentum spectrum is one of the key observables that could unravel the nature of the dark matter couplings to the Standard Model from monojet probes [6, 7]. In this work, we study the effect of derivative and non-derivative couplings between the Standard Model and the new physics sector on the monojet kinematics. Our preliminary results, including only 8 TeV LHC data, appeared in the proceedings of the "Les Houches 2015 – Physics at TeV colliders" workshop [8].

Models with derivative couplings are motivated by new physics setups featuring pseudo-Nambu-Goldstone bosons (pNGBs), *i.e.* light scalar fields connected to the spontaneous breaking of a global symmetry at an energy scale f. More concretely, this class of models includes composite Higgs scenarios where the set of pNGBs involves the Higgs boson and possibly extra dark scalar particles [9–14]. In this case, the pNGB shift symmetry indeed only allows for derivative (momentum-dependent) pNGB interactions suppressed by powers of the scale f. An explicit weak breaking of the shift symmetry, parameterized

by a small coupling strength ϵ, is however necessary in order to induce pNGB masses, which subsequently generates additional non-derivative momentum-independent couplings proportional to ϵ/f. In this work, we rely on a simplified effective field theory approach where the form of the Lagrangian is inspired by such pNGB setups, with all specific and model-dependent assumptions for the new physics masses and couplings being, however, relaxed. As already pointed out in the literature, this effective Lagrangian approach is appropriate for interpreting LHC missing energy signatures within frameworks featuring light dark matter particles interacting with the Standard Model via non-renormalizable derivative operators [13, 14].

Most ultraviolet-complete models of dark matter involve additional particles, potentially carrying Standard Model quantum numbers. Although dedicated LHC searches could detect such additional states, we consider a simple setup where the only new states that are accessible at the LHC are the dark matter particle and (sometimes) the mediator connecting the Standard Model and the dark sector. More specifically, we first consider an invisible sector solely comprised of a Standard Model-singlet real scalar field η which is taken to be odd under a $\mathcal{Z}_2$ discrete symmetry. The Standard Model fields are then chosen to be even under the same $\mathcal{Z}_2$ symmetry, which forbids the decay of the η particle into any ensemble of Standard Model states and renders it a potential dark matter candidate. In a minimal scenario, the mediator is taken to be the Standard Model Higgs field H that interacts with η via both a renormalizable quartic coupling and a non-renormalizable derivative coupling. This framework, however, turns out to be strongly constrained by LHC measurements of the Higgs boson properties. As an alternative we therefore consider a slightly extended setup where we additionally introduce a real gauge-singlet $\mathcal{Z}_2$-even scalar mediator particle s, a choice which allows us to avoid these constraints. While s couples to the dark sector both through a derivative (dimension-five) and a non-derivative renormalizable operator, it is connected to the Standard Model only through a (potentially loop-induced) dimension-five operator involving gluon field strength bilinears. This simple model not only reproduces the observed dark matter abundance of the universe but also, assuming that momentum-dependent interactions dominate, can evade the direct detection constraints.

In this paper, we first provide details of our theoretical framework in Section 2 and then examine the LHC constraints stemming from the monojet analysis performed by the ATLAS collaboration for proton-proton collisions at a center-of-mass energy of 13 TeV with 3.2 fb^{-1} in Section 3. We assess the effects of momentum-dependent and momentum-independent dark matter couplings on monojet distributions and derive the corresponding bounds for both cases. Dijet searches for the mediator s at past and present colliders are also taken into account and discussed, and we finally entertain the possibility that the η particle is responsible for the measured dark matter density in the Universe. In this spirit, we investigate the dependence of the relic abundance and the direct dark matter detection constraints on the model parameters. Our findings are summarized in Section 4, and technical details on the range of validity of our effective description based on perturbative unitarity arguments are presented in Appendix A.

2 Theoretical framework and constraints

2.1 The minimal scenario: the Higgs portal

In order to study the impact of derivative and non-derivative couplings of dark matter to the Standard Model, we first consider a minimal setup involving both momentum-dependent and momentum-independent couplings of the dark matter particle. We impose that the dark matter only couples to the Higgs field, which plays the role of the mediator.

We supplement the Standard Model by a gauge-singlet real scalar field η that is chosen odd under a $\mathcal{Z}_2$ symmetry, where in contrast the Standard Model fields are taken to be even. The η particle then only interacts with the Standard Model through couplings to the Higgs doublet H, such that the model Lagrangian reads

$$\mathcal{L}_\eta = \mathcal{L}_{\rm SM} + \frac{1}{2}\partial_\mu\eta\partial^\mu\eta - \frac{1}{2}\mu_\eta^2\eta^2 - \frac{1}{4}\lambda_\eta\eta^4 - \frac{1}{2}\lambda\eta^2 H^\dagger H + \frac{1}{2f^2}(\partial_\mu\eta^2)\partial^\mu(H^\dagger H) \ . \tag{2.1}$$

This Lagrangian contains renormalizable operators compatible with the $\mathcal{Z}_2$ symmetry ($\eta \to -\eta$) and a dimension-six operator involving derivatives. While several other non-derivative dimension-six operators are allowed by the model symmetries, these are not expected to have a significant impact on the monojet analysis. As the effect of these operators is negligible for our purposes, we have omitted these in our parameterization of Eq. (2.1). In the context of composite Higgs models, the scalar field η may be a pNGB and f its decay constant. The theoretical motivations for this minimal model and the resulting dark matter phenomenology are described in Ref. [9]. Further related studies are also available in the literature [10–12].

After electroweak symmetry breaking, the part of the Lagrangian containing the interactions of η with the physical Higgs boson h is given by

$$\mathcal{L}_\eta \supset -\frac{1}{4}(v+h)^2\left(\lambda\eta^2 + \frac{1}{f^2}\partial_\mu\partial^\mu\eta^2\right) \ , \tag{2.2}$$

and the η mass m_η satisfies

$$m_\eta^2 = \mu_\eta^2 + \lambda v^2/2 \ . \tag{2.3}$$

The trilinear scalar interaction in Eq. (2.2) yields monojet events at the LHC via, for instance, the gluon fusion process $gg \to gh^{(*)} \to g\eta\eta$, while the quartic interactions give rise to mono-Higgs events $gg \to h^* \to h\eta\eta$. When $2m_\eta < m_h$, the Higgs boson is produced on-shell and the strength of the derivative interaction vertex is proportional to $p_h^2/f^2 = m_h^2/f^2$, with p_h being the final-state Higgs boson four-momentum. The momentum-dependence reduces to a constant, so that momentum-dependent interactions become indistinguishable from their momentum-independent counterparts. In this regime, bounds from monojet searches are found to be weaker than the constraints stemming from the Higgs invisible width results [15–17],

$$\Gamma(h\to\eta\eta) = \frac{v^2}{32\pi m_h}\left(\frac{m_h^2}{f^2} - \lambda\right)^2\sqrt{1-\frac{4m_\eta^2}{m_h^2}}\,\theta(m_h^2-4m_\eta^2) \lesssim 0.15\Gamma_h^{\rm SM} \simeq 0.7 \text{ MeV} \ , \tag{2.4}$$

at the 95% confidence level.

We therefore focus on the complementary kinematic region where $2m_\eta > m_h$. The monojet signal arises from off-shell Higgs-boson production, and the derivative interactions of the η particle result in a strong momentum dependence at the differential cross-section level. The subsequent differences in the jet transverse momentum distribution could allow us to discriminate derivative from non-derivative dark matter couplings. This however comes at the price of a suppression of the monojet signal, since the relevant partonic cross-section $\hat{\sigma}$ depends on the virtuality of the Higgs boson p_h^2 as

$$\hat{\sigma}(gg \to gh^* \to g\eta\eta) \propto \frac{\theta(p_h^2 - 4m_\eta^2)}{(p_h^2 - m_h^2)^2 + \Gamma_h^2 m_h^2} \left(\frac{p_h^2}{f^2} - \lambda\right)^2 \sqrt{1 - \frac{4m_\eta^2}{p_h^2}} \,, \tag{2.5}$$

where Γ_h denotes the Higgs total width. The denominator is clearly larger in the region where the Higgs is off-shell, or equivalently when $p_h^2 > 4m_\eta^2 > m_h^2$.

A preliminary monojet analysis within the considered theoretical framework has recently been performed [18], and the collider signatures of this off-shell Higgs portal model are discussed in Ref. [19]. Our numerical analysis however indicates that in the light of current experimental data, the monojet signal is too weak to be observed at the LHC. The precise determination of the Higgs-boson mass and the important LHC constraints on its production cross-section and decay width indeed result in tight bounds on the free parameters of the model,

$$m_\eta \gtrsim m_h/2, \qquad \lambda \lesssim 1, \qquad f \gtrsim 500 \text{ GeV} - 1 \text{ TeV} \,, \tag{2.6}$$

where the latter bound applies to models in which the Higgs is a composite pNGB. As a consequence, the total monojet cross-section after including a selection on the jet transverse momentum of $p_T^{\text{jet}} > 20$ GeV is always smaller than 1 fb and 0.5 fb when only momentum-dependent and momentum-independent couplings are allowed, respectively, for a center-of-mass energy of $\sqrt{s} = 13$ TeV.

2.2 A pragmatic scenario with a scalar singlet mediator

Given the tight constraints discussed in the previous section, we extend our framework to analyse a scenario less severely constrained by data. In addition to the dark matter field η we introduce a second scalar mediator field s, chosen to be even under the $\mathcal{Z}_2$ symmetry and a singlet under the Standard Model gauge symmetries. We moreover impose that the scalar potential does not spontaneously break the $\mathcal{Z}_2$ symmetry, or equivalently that η does not acquire a non-vanishing vacuum expectation value (vev). We further demand, without any loss of generality, that the vev of the s field vanishes as the latter could always be absorbed in a redefinition of the couplings.

The relevant Lagrangian is given by

$$\begin{aligned} \mathcal{L}_{\eta,s} = \mathcal{L}_{\text{SM}} &+ \frac{1}{2}\partial_\mu \eta \partial^\mu \eta - \frac{1}{2} m_\eta^2 \eta\eta + \frac{1}{2}\partial_\mu s \partial^\mu s - \frac{1}{2} m_s^2 ss \\ &+ \frac{c_{s\eta} f}{2} s\eta\eta + \frac{c_{\partial s\eta}}{f}(\partial_\mu s)(\partial^\mu \eta)\eta + \frac{\alpha_s}{16\pi}\frac{c_{sg}}{f} s G^a_{\mu\nu} G^{a\mu\nu} \,, \end{aligned} \tag{2.7}$$

where we include an effective coupling between the s and gluon fields. Consequently, the mediator can be produced at the LHC via gluon fusion and can give rise to a monojet signal via the mechanism $gg \to gs^* \to g\eta\eta$. In ultraviolet-complete models, this c_{sg} coupling can be generated by additional new physics. For example, in a scenario featuring a vector-like color-triplet fermion ψ of mass $M_\psi \gg m_s$ that interacts via a Yukawa interaction $y_\psi \bar{\psi}\psi s$, triangle loop-diagram contributions induce $c_{sg} = (4/3)(y_\psi f/M_\psi)$. Finally, the non-derivative coupling $c_{s\eta}$ governs the momentum-independent interaction of the two scalars s and η and, for a given value of the scale f, the derivative coupling $c_{\partial s\eta}$ controls the strength of the leading momentum-dependent interactions.

The Lagrangian given in Eq. (2.7) only includes interactions that are relevant to our analysis, and the considered dimension-five operator is the unique independent derivative dimension-five operator inducing an interaction between s and η. The model can hence be described in terms of six parameters,

$$m_s, \quad m_\eta, \quad f, \quad c_{s\eta}, \quad c_{\partial s\eta} \quad \text{and} \quad c_{sg}. \tag{2.8}$$

Strictly speaking, only five of these parameters are independent as one can always choose $c_{\partial s\eta} = 1$ and determine the strength of the momentum-dependent interaction by varying f. This choice is motivated by models where s, η and the Higgs boson are pNGBs associated with the spontaneous breaking of a global symmetry at a scale f and where $c_{\partial s\eta}$ is expected to be of order one. In this case, the f parameter is constrained by precision Higgs and electroweak data that roughly imposes $f \gtrsim 500$ GeV $-$ 1 TeV [20]. In our numerical analysis of Section 3, we consider four representative values for the s particle mass, $m_s = 50$ GeV, 250 GeV, 500 GeV and 750 GeV, which allows us to cover a wide range of mediator masses.

2.3 Constraints on the parameters of the model

The model can be constrained in a number of ways. In particular, searches for dijet resonances could be promising since a singly-produced mediator via gluon fusion often decays back into a pair of jets ($gg \to s^{(*)} \to gg$). For the case where η is a viable dark matter candidate, the model should in additional yield a relic density in agreement with Planck measurements and satisfy direct dark matter detection bounds. Before getting into a detailed investigation of these constraints, we first study some properties of the model in order to understand the bounds that can be expected from collider, cosmological and theoretical considerations. A complete set of numerical results is then presented in Section 3.

From the Lagrangian given in Eq. (2.7), the partial decay widths of the s particle into gluon and η pairs are calculated to be

$$\Gamma(s \to gg) = \frac{\alpha_s^2 c_{sg}^2 m_s^3}{128\pi^3 f^2} \ , \tag{2.9}$$

$$\Gamma(s \to \eta\eta) = \frac{f^2}{32\pi m_s}\left(c_{\partial s\eta}\frac{m_s^2}{f^2} + c_{s\eta}\right)^2 \sqrt{1 - \frac{4m_\eta^2}{m_s^2}}\ \theta(m_s^2 - 4m_\eta^2) \ , \tag{2.10}$$

in agreement with results obtained using the decay module of FeynRules [21, 22]. For the coupling values adopted in our analysis, the total width Γ_s is always small. This implies

that the narrow width approximation can be used for any cross-section calculation involving a resonant s-contribution. The s-induced dijet cross section can hence be expressed as

$$\sigma(pp \to s \to gg) = \int_0^1 \mathrm{d}x_1 \int_0^1 \mathrm{d}x_2 \; f_g(x_1, m_s) f_g(x_2, m_s) \frac{\alpha_s^2 c_{sg}^2 m_s^2}{1024\pi f^2} \; \delta(\hat{s} - m_s^2) \mathrm{BR}\Big(s \to gg\Big) \; , \tag{2.11}$$

where $\sqrt{\hat{s}}$ denotes the partonic center-of-mass energy and $f_g(x, \mu)$ the universal gluon density that depends on the longitudinal momentum fraction x of the gluon in the proton and the factorization scale μ. For the considered values of m_s, the most stringent dijet constraints arise from Sp$\bar{\text{p}}$S [23] and Tevatron [24] data which provides upper limits on the new physics cross section σ for mediator masses of 140 – 300 GeV and 200 – 1400 GeV respectively. In comparison, the LHC Run I results further extend the range of covered mediator masses up to 4.5 TeV [25, 26]. For $f = 1000$ GeV, we find that c_{sg} values up to about 100 (which corresponds to an effective coupling of about 10^{-3}) are allowed independently of the other parameters, and we adopt this upper limit henceforth.

Turning our attention to the dark matter phenomenology, we first study the η relic abundance $\Omega h^2|_\eta$. This is numerically computed in Section 3 with the MicrOmegas package [27], in which we have implemented our model via FeynRules [22]. An approximate expression describing the relevant total thermally-averaged annihilation cross section $\langle \sigma v \rangle$ can nonetheless be derived analytically. Restricting ourselves to the leading S-wave contribution and ignoring all possible special kinematic configurations featuring, *e.g.*, intermediate resonances, the thermally-averaged cross section associated with η annihilation into a pair of gluons is given by

$$\langle \sigma v \rangle_{gg} \simeq \frac{\alpha_s^2 c_{sg}^2 m_\eta^2 \left(c_{s\eta} f^2 + 4 c_{\partial s\eta} m_\eta^2\right)^2}{16\pi^3 f^4 \left(m_s^2 - 4m_\eta^2\right)^2} \; . \tag{2.12}$$

In the case where $m_\eta > m_s$, an additional $2 \to 2$ annihilation channel contributes, $\eta\eta \to ss$, whose leading S-wave contribution reads

$$\langle \sigma v \rangle_{ss} \simeq \frac{\sqrt{1 - \frac{m_s^2}{m_\eta^2}} \left(c_{\partial s\eta} m_s^2 + c_{s\eta} f^2\right)^4}{16\pi f^4 m_\eta^2 \left(m_s^2 - 2m_\eta^2\right)^2} \; . \tag{2.13}$$

We impose the requirement that the η relic density satisfies the upper limit [28]

$$\Omega h^2|_\eta \leq \Omega h^2|_{\text{exp}} = 0.1188 \pm 0.0010 \, . \tag{2.14}$$

Assuming a standard thermal freeze-out mechanism, and ignoring singular parameter space regions such as resonances, the dark matter relic density does not depend strongly on whether $m_\eta > m_s/2$ or $< m_s/2$. This condition is, however, crucial for the LHC: monojet searches can typically only reach couplings that correspond to thermal self-annihilation cross sections once the mediator can be produced and decay on-shell. Instead, in the off-shell regime, the LHC tends to probe parameter space regions where the dark matter abundance lies below $\Omega h^2|_{\text{exp}}$ [29], but there are exceptions [30]. Finally, regardless of the

momentum-dependent or -independent nature of the dark matter interactions the dominant contribution to the dark matter annihilation comes from the S-wave.

Direct detection searches yield additional constraints on the phenomenologically viable regions of the model parameter space. These however do not constrain the strength of the momentum-dependent interactions, as the corresponding scattering cross section is proportional to the dark matter-nucleus momentum transfer which is very small compared to the mediator mass. On the other hand, the momentum-independent couplings in Eq. (2.7) lead to an effective interaction between η particles and gluons,

$$\mathcal{L}_{\eta g} = f_G \, \eta^2 \, G_{\mu\nu} G^{\mu\nu} \qquad \text{with} \qquad f_G = \frac{\alpha_s c_{sg} c_{s\eta}}{32\pi} \frac{1}{m_s^2} \, . \tag{2.15}$$

The spin-independent dark matter scattering cross section $\sigma_{\rm SI}$ is then found to take the form [31, 32]

$$\sigma_{\rm SI} = \frac{1}{\pi} \left(\frac{m_\eta m_p}{m_\eta + m_p} \right)^2 \left| \frac{8\pi}{9\alpha_s} \frac{m_p}{m_\eta} f_G f_{TG} \right|^2 \, , \tag{2.16}$$

where the term inside the brackets corresponds to the DM-nucleon reduced mass, and the squared matrix element depends on the gluon form factor f_{TG}. The latter is derived from the quark form factors f_{Tq} [33],

$$f_{TG} = 1 - \sum_{q=u,d,s} f_{Tq} \, , \tag{2.17}$$

for which we take the values $f_{Tu} = 0.0153$, $f_{Td} = 0.0191$ and $f_{Ts} = 0.0447$ [34]. The above expression for f_{TG} would change if additional couplings between the mediator s and quarks were introduced. Our predictions for $\sigma_{\rm SI}$ are compared, in the next section, to limits extracted from LUX data [35][1].

Finally, additional restrictions can also be imposed on the model from perturbative unitarity requirements. For a given process, the effective Lagrangian in Eq. (2.7) is indeed expected to provide an accurate description of the underlying physics only as long as the typical momentum involved lies below a cutoff scale which we have so far kept unspecified. This scale can be deduced rigorously on a model-by-model basis, but its minimal acceptable value can be estimated without referring to any specific ultraviolet completion. By enforcing the S matrix to be perturbatively unitary, we ensure that calculations performed on the basis of the Lagrangian of Eq. (2.7) provide reliable predictions [37–39].

We provide the details of the calculation in Appendix A, where we show that perturbative unitarity of the $gg \to \eta\eta$ scattering amplitude imposes the constraints

$$\kappa_{\rm MI} < \frac{64\sqrt{2}\pi^2 (1 - \frac{m_s^2}{Q^2})}{\alpha_s \left(1 - \frac{4m_\eta^2}{Q^2}\right)^{1/4}} \, , \tag{2.18}$$

[1] While this work was being completed, the LUX collaboration has updated their results on the basis of 332 live days of exposure [36]. We do not include the latest limits in our analysis. Although more constraining, the new LUX results do not imply significant differences in the allowed region of the parameter space.

where $\kappa_{\rm MI} = c_{s\eta} c_{sg}$ and

$$\kappa_{\rm MD} < \frac{64\sqrt{2}\pi^2 f^2 (Q^2 - m_s^2)}{\alpha_s Q^4 \left(1 - \frac{4m_\eta^2}{Q^2}\right)^{1/4}} \,, \tag{2.19}$$

with $\kappa_{\rm MD} = c_{\partial s\eta} c_{sg}$. In typical hadron collider processes like those occuring at the LHC, the scale Q^2 varies from one event to another. In order to simplify the discussion, we judiciously focus on large values of Q^2 that are relevant for the high-energy tail of the differential distributions where the effective theory is expected to break down. Considering typical missing transverse-momentum distributions related to monojet events and the current LHC luminosity, the tail of the distribution extends to $|Q| \sim 2$ TeV while most events relevant for the extraction of LHC constraints feature a missing transverse energy in the [700, 1500] GeV range. In the next section, unitarity bounds are therefore computed for the conservative choice $|Q| = 2$ TeV.

3 Numerical results

We now estimate the constraining power of monojet searches both in the case of momentum-dependent and momentum-independent interactions. For simplicity, we consider scenarios featuring either momentum-independent ($c_{\partial s\eta} = 0$) or momentum-dependent ($c_{s\eta} = 0$) couplings, and we set the composite scale f to 1 TeV. The mediator coupling to the gluon field strength tensor is fixed to $c_{sg} = 10$ and 100, as allowed by the dijet bounds discussed in Section 2.2. We finally discuss the complementarity between theory, collider and cosmological constraints.

3.1 Analysis setup

In order to evaluate the LHC sensitivity to our model via monojet probes, we compare our theoretical predictions to official ATLAS results based on early 13 TeV data at an integrated luminosity of 3.2 fb^{-1} [3]. This is achieved via an implementation of the analysis of Ref. [3] in the MadAnalysis 5 framework [40, 41]. Details on our code and its validation are publicly available on Inspire [42] and within the MadAnalysis 5 Public Analysis Database [43] [2]. Our recasted analysis is in agreement with the ATLAS official results for well-defined event samples at the 5% level, and we have also compared, for consistency, our results to those obtained when using LHC Run I data [8].

The analysis under consideration preselects events featuring one final-state hard jet with a transverse-momentum p_T larger than 250 GeV and a pseudorapidity satisfying $|\eta| < 2.4$, as well as at most four jets with $p_T > 30$ GeV and $|\eta| < 2.8$. Moreover, each jet is required to be azimuthally separated from the missing momentum by an angle $\Delta\phi > 0.4$, and events exhibiting muons or electrons with a transverse momentum greater than 10 GeV and 20 GeV respectively are vetoed. Preselected events are then categorized into seven inclusive and six exclusive signal regions. The seven inclusive regions are defined by seven overlapping selections on the missing transverse energy, demanded to be larger than 250, 300, 350, 400, 500, 600 and 700 GeV. The same thresholds are further used to define six

[2] https://madanalysis.irmp.ucl.ac.be/wiki/PublicAnalysisDatabase.

missing energy bins [250,300], [300,350], [350,400], [400,500], [500,600] and [600,700] GeV, which form the six exclusive signal regions.

In order to perform our study, we have implemented the model described in Section 2.2 in the FeynRules [22] package, and generated a UFO library [44] that we have imported into MadGraph5_aMC@NLO [45]. Hard-scattering events describing the $pp \to \eta\eta j$ process (with an 80 GeV selection threshold on the jet p_T) have been generated for a center-of-mass energy of 13 TeV and matched to the parton showering and hadronization infrastructure of Pythia 6 [46]. The events are then processed by Delphes 3 [47] for a fast detector simulation using a tuned parameterization of the ATLAS detector and the Fastjet program [48] for jet reconstruction by means of the anti-k_T algorithm [49] with an R-parameter set to 0.4. Finally, the MadAnalysis 5 program is used to handle the event selection and to compute the associated upper limit at the 95% confidence level (CL) on the signal cross section according to the CLs technique [50, 51]. Although the considered analysis contains 13 signal regions, the upper bound on the cross section (interpreted at leading order) is determined only from the region that is expected to be the most sensitive. This region is determined using the background rate, its uncertainty and the observed number of events reported by the ATLAS collaboration.

For discrete choices of the mediator mass $m_s = 50$, 250, 500 and 750 GeV, we scan over various ranges of the dark matter mass with $2m_\eta > m_s$. Since only one of the $c_{s\eta}$ or $c_{\partial s\eta}$ parameters are taken to be non-zero at a time, the computed cross section upper limits only depend on the kinematics of the events and not on the overall rate. The results are thus independent of the actual values of the $c_{s\eta}$, $c_{\partial s\eta}$ and c_{sg} parameters, and we have consequently fixed ($c_{s\eta}$, $c_{\partial s\eta}$) to the nominal values (1, 0) and (0, 1). This choice enables an easy rescaling of the monojet cross section when different values of the input parameters are chosen and a straightforward derivation of limits on the momentum-dependent and momentum-independent interactions for a given set of masses and couplings.

In addition, we have also evaluated the LHC sensitivity to our model for a luminosity of 300 fb^{-1}, this time using Pythia 8 [52] for the parton showering and hadronization of the signal samples, along with efficiency factors and smearing functions aimed at reproducing the performance of the ATLAS detector during the first run of the LHC [53]. Thanks to the higher statistics and the different shape of the missing energy distribution for signal and background, the optimal sensitivity to the signal is expected for tighter missing energy requirements than those adopted in Ref. [3], thus motivating extending the number of signal regions. This, however, requires the extrapolation of the predictions for the expected Standard Model background and the associated uncertainties.

The 3.2 fb^{-1} monojet publication of ATLAS provides the Standard Model expectation for the missing transverse-energy distribution [3], so that the latter can be used to extract the expected number of background events $N_{\rm bg}$ for 300 fb^{-1}. The estimation of the systematic uncertainties $\Delta N_{\rm bg}$ is however luminosity-dependent due to an extrapolation of the dominant Z+jets and W+jets backgrounds from the number of data events observed in appropriate control regions to the signal regions. We consequently parametrise $\Delta N_{\rm bg}$ as

$$\Delta N_{\rm bg}^2 = \left(k_1 \sqrt{N_{\rm bg}}\right)^2 + \left(k_2 N_{\rm bg}\right)^2 . \tag{3.1}$$

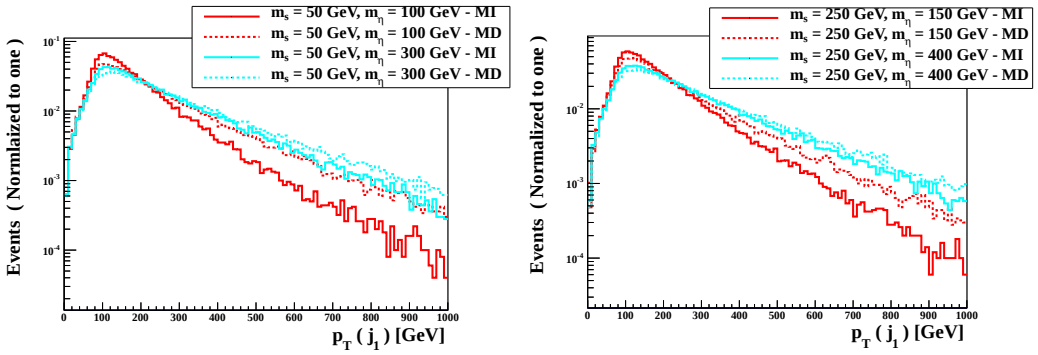
m_s = 50 GeV, m_η = 100 GeV - MI
m_s = 50 GeV, m_η = 100 GeV - MD
m_s = 50 GeV, m_η = 300 GeV - MI
m_s = 50 GeV, m_η = 300 GeV - MD
Events (Normlaized to one)
p_T (j_1) [GeV]
m_s = 250 GeV, m_η = 150 GeV - MI
m_s = 250 GeV, m_η = 150 GeV - MD
m_s = 250 GeV, m_η = 400 GeV - MI
m_s = 250 GeV, m_η = 400 GeV - MD
Events (Normalized to one)
p_T (j_1) [GeV]

Figure 1. Normalized distributions in the transverse momentum of the leading jet assuming a perfect detector. We consider a mediator mass of 50 GeV and 250 GeV in the left and right panels respectively, and a dark matter mass of 100 GeV and 300 GeV (left panel) or 150 GeV and 400 GeV (right panel). The solid lines reflect scenarios featuring momentum-independent (MI) interactions while the dashed lines correspond to scenarios featuring momentum-dependent (MD) interactions.

The first term on the right-hand side represents the statistical error on the number of events observed in the control regions and is controlled by the k_1 parameter, while the second term consists of the systematic uncertainties connected to the extrapolation procedure from the control region to the signal regions and is driven by the k_2 parameter. The ATLAS analysis finds the latter to be slowly varying with the missing transverse-energy selection and is of the order of a few percent [3]. We adopt the choice of $k_1 = 1.51$ and $k_2 = 0.043$, which parametrize the ATLAS results of Ref. [3] at the percent level, and calculate 95% CL upper limits on the signal cross-section for overlapping signal regions defined by minimum requirements on the missing transverse energy varying in steps of 100 GeV between 500 and 1400 GeV. The statistical procedure relies on a Poisson modelling with Gaussian constraints using the CLs prescription and the asymptotic calculator implemented in the RooStat package [54]. The lowest upper limit on the fiducial production cross section (with a constraint on the jet transverse momentum of $p_T > 80$ GeV) is then taken to be the final result.

3.2 Bounds derived from LHC monojet data

As a first illustration of the differences between scenarios featuring momentum-independent and momentum-dependent interactions, we show the leading jet p_T distributions obtained with MadAnalysis 5 for the representative mass combinations $(m_s, m_\eta) = (50, 100/300)$ GeV and $(m_s, m_\eta) = (250, 150/400)$ GeV in the left and right panels of Figure 1 respectively. Focusing on the shapes of the distributions that have been normalized to one, one observes that momentum-dependent interactions induce a harder jet p_T spectrum. As a result, one expects that a larger fraction of events would pass a monojet selection when momentum-dependent interactions are present. For instance, choosing $c_{sg} = 100$, $f = 1$ TeV and either $c_{\partial s\eta} = 2.5$ in the momentum-dependent case or $c_{s\eta} = 0.5$ in the momentum-independent case we obtain, in both scenarios, a fiducial cross section of 2.9 pb

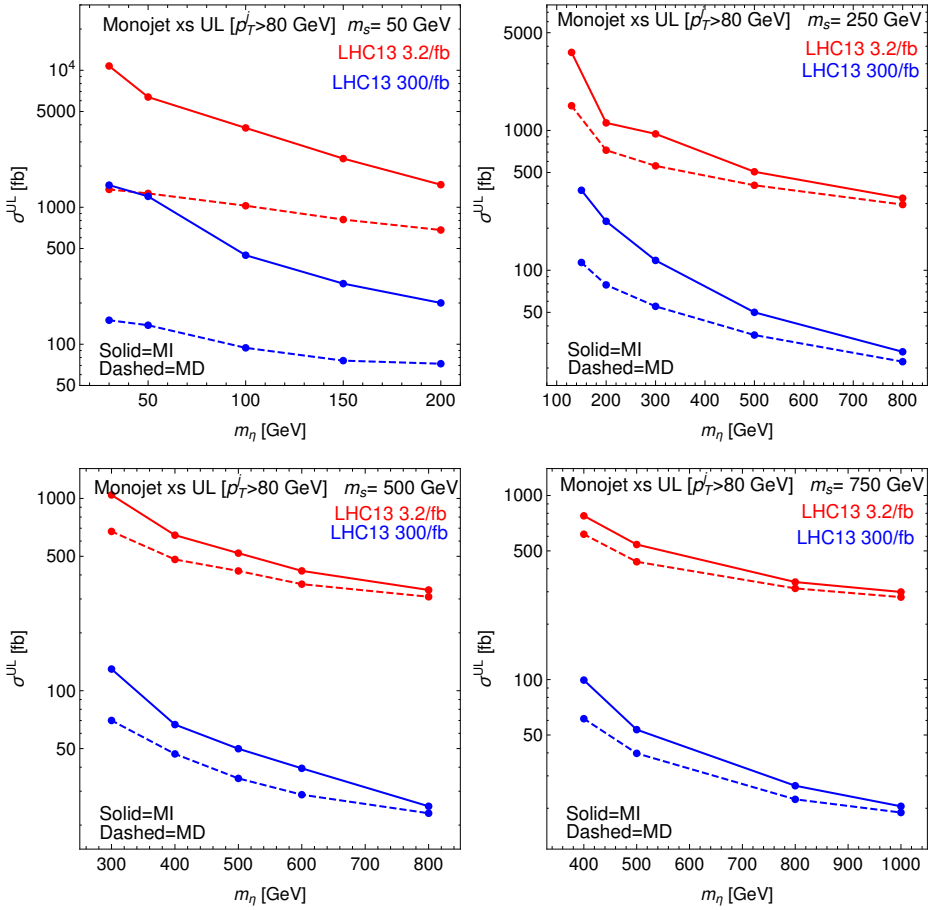

Figure 2. 95% CL upper limits (UL) on the monojet production fiducial cross section (that includes a generator-level selection of $p_T > 80$ GeV on the leading jet). We consider proton-proton collisions at a center-of-mass energy of 13 TeV with an integrated luminosity of 3.2 fb^{-1} (recasting, red lines) and 300 fb^{-1} (projections, blue lines) for $m_s = 50$ GeV (top left), 250 GeV (top right), 500 GeV (bottom left) and 750 GeV (bottom right) as a function of m_η. The solid lines correspond to the momentum-independent case, whereas the dashed lines correspond to the momentum-dependent case.

once an 80 GeV generator-level selection on the leading jet p_T is enforced. The efficiency associated with a transverse-momentum selection of $p_T > 300$ GeV on the leading jet is, however, relatively larger by about 50% in the momentum-dependent case. The difference between the two scenarios is significantly reduced for larger dark matter masses.

As explained in Section 3.1, for a given value of m_s the constraints that can be derived from LHC dark matter searches only depend on m_η, since in the relevant subprocesses the mediator has to be off-shell. In Figure 2, we present the upper limits on the monojet cross section at the LHC, $\sigma^{\rm UL}(pp \to \eta\eta j)$, with a generator-level selection on the transverse momentum of the leading jet of $p_T > 80$ GeV. Existing constraints extracted from 3.2 fb^{-1} of 13 TeV LHC collisions are depicted by red lines for the momentum-independent (solid) and dependent (dashed) cases. As anticipated, the cross sections excluded at the 95% CL are

significantly smaller in the momentum-dependent setup than in the moment-independent one, so that the former is more efficiently constrained than the latter. We additionally observe that the exclusion bounds become stronger with increasing m_η. As long as enough phase space is available, larger η masses imply a larger amount of missing energy so that the signal regions of the monojet analysis are more populated and stronger limits can be derived, as shown in the figure.

Our results confirm the findings of Figure 1, the differences between the momentum-independent and momentum-dependent cases being maximal for small values of m_η. Eventually, for dark matter masses of about 1 TeV, the limits become identical for both cases although the LHC loses its sensitivity for such heavy dark matter scenarios.

We also report in Figure 2 projections for 300 fb^{-1} of LHC collisions at a center-of-mass energy of 13 TeV. The blue solid and dashed lines respectively represent the momentum-independent and momentum-dependent cases. We observe a behavior that is similar to the lower luminosity one, although it is now driven by the additional higher missing-energy requirements. In the relevant bins, the signal acceptance is again found to be higher for the momentum-dependent dark matter coupling case, so that the corresponding exclusion bounds are stronger. Moreover, the two classes of dark matter operators can still only be distinguished up to a given dark matter mass, which is nonetheless larger than for lower luminosities.

3.3 Complementarity of collider, cosmological and theoretical considerations

In order to estimate the regions of the model parameter space that are viable with respect to current data, we investigate the interplay between the LHC monojet bounds presented in the previous section and the dark matter and theoretical considerations discussed in Section 2.2. Assuming momentum-independent dark matter interactions, the LUX results exclude the spin-independent direct detection cross section predicted by Eq. (2.16) in the entire parameter space region accessible with the 13 TeV LHC monojet results. More precisely, for a dark matter mass of 50 GeV that is close to the LUX sensitivity peak and for the minimal $c_{sg} = 10$ choice, the maximum $c_{s\eta}$ allowed values are of the order of 1.2×10^{-3}, 0.03, 0.13 and 0.28 for $m_s = 50$, 250, 500 and 750 GeV respectively. Increasing the dark matter mass to a slightly higher value of 200 GeV that is still within the LHC reach, these numbers increase to 0.008, 0.2, 0.5 and 0.9 [3]. Therefore, in the momentum-independent case, an observable monojet signal could be explained only by missing energy unrelated to dark matter. Thus, in the following, we show the constraint from the dark matter relic density only for the momentum-dependent case.

In Figures 3 and 4 we superimpose constraints arising from the 13 TeV LHC monojet search results and the corresponding projections (red and blue lines respectively) on those obtained by imposing the relic density bound of Eq. (2.14) (the latter for the momentum-dependent case only), assuming a standard thermal freeze out dark matter scenario. The bounds on the $c_{s\eta}$ coupling are stronger for larger f values while those on the $c_{\partial s\eta}$ parameter are weaker. In the shaded regions, $\eta\eta$ annihilation is not efficient enough, so that the

[3] These numbers assume that the local dark matter density is $\rho_0 = 0.3$ GeV cm^{-3}.

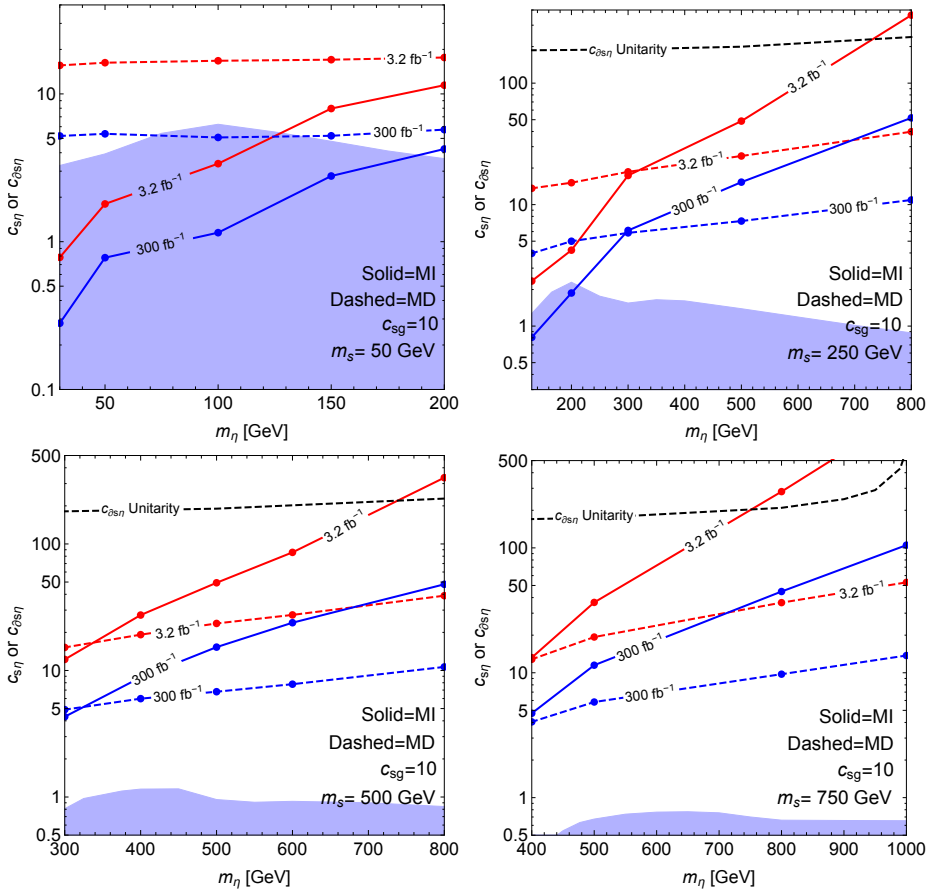

Figure 3. Constraints on the c_i couplings of Eq. (2.7) driven by monojet searches. The red lines depict constraints from existing 3.2 fb^{-1} of data whereas blue ones correspond to predictions for an integrated luminosity of 300 fb^{-1}. We fix $f = 1$ TeV, $m_s = 50$ GeV (top left), 250 GeV (top right), 500 GeV (bottom left) and 750 GeV (bottom right) and the results are represented as functions of m_η for $c_{sg} = 10$. The shaded regions correspond to momentum-dependent coupling values for which the universe is overclosed, while above the black lines the perturbative unitarity of the effective theory is lost. The solid and dashed lines correspond to the momentum-independent (MI) and dependent (MD) cases respectively.

Universe is overclosed. Along the borders of these regions, the relic density limit is exactly reproduced, the shape of these borders being fairly well described by the approximate results of Eq. (2.12) and Eq. (2.13). In the un-shaded region, the predicted abundance is smaller than the observed Planck value.

Since in our parameter space scan, no resonant configuration can occur, the $c_{\partial s\eta}$ values satisfying the dark matter abundance bounds vary relatively mildly with the dark matter and mediator masses. The minor apparent features (especially in the $m_s = 250$ GeV and 500 GeV scenarios) that can be observed are related to the opening of the additional dark matter annihilation channel into s pairs. For our choices of parameters, however, this channel only contributes subleadingly to the relic density, its maximal impact being found

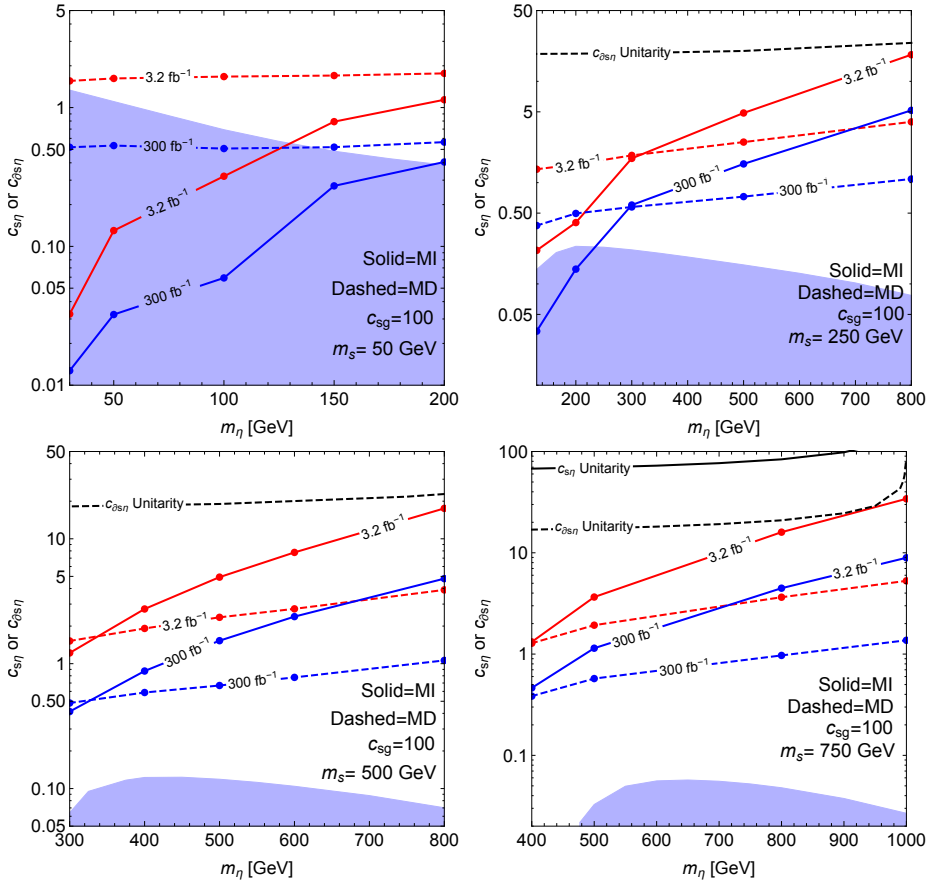

Figure 4. Same as in Figure 3 but for $c_{sg} = 100$.

to be of the order of 15%. The annihilation cross section hence approximately scales as $(c_{\partial s\eta} \times c_{sg})^2$, so that a smaller value of c_{sg} implies almost proportionally larger allowed values for $c_{\partial s\eta}$.

We also include in the figures the perturbative unitarity limit of validity of our effective parameterization (black dashed line) choosing $|Q| = 2$ TeV in Eq. (2.19). For $c_{sg} = 10$ the perturbative unitarity bound reads $c_{\partial s\eta} \lesssim 190$ in the momentum-dependent case, and $c_{s\eta} \lesssim 760$ in the momentum-independent case. This bound depends weakly on m_s and m_η, however it is proportional to $1/c_{sg}$, as observed on comparing Figure 3 with Figure 4. We observe that although the unitarity limits do exhibit some overlap with the current and projected LHC reach, our effective description is consistent over most of the parameter space.

Our findings show that existing monojet constraints are not yet strong enough to probe regions of parameter space where η can account for the entire dark matter energy density of the Universe. We therefore recover the fairly well-known result that in the "off-shell" regime of dark matter models, the LHC tends to be sensitive to dark matter candidates for which the relic density is underabundant [55, 56]. On the other hand, collider searches

probe large values of the $s\eta\eta$ coupling while the Planck results instead constrain small values, where the Universe tends to be overclosed. In this sense, there is an interesting complementarity between collider and cosmological measurements. Besides, we observe that for an integrated luminosity of 300 fb^{-1}, the LHC will be able to access a part of the low-mass region of our model where the observed dark matter abundance can be exactly reproduced, for dark matter masses up to about 140 GeV. Whether or not it will be able to actually *distinguish* between the two scenarios will be the subject of forthcoming work. Another remark is related to the fact that our results are valid regardless of the stability of the η states at cosmological timescales. In other words, letting aside model-building considerations, our analysis holds for metastable η particles as well, as long as they do not decay within the LHC detectors.

4 Conclusion

Momentum-dependent couplings between dark matter and the Standard Model are well-motivated both from a theoretical and a phenomenological perspective. Indeed, broad classes of ultraviolet-complete dark matter models predict effective derivative operators at low energy, in particular whenever the dark matter particle is an approximate Goldstone boson of the underlying theory. This is quite natural in the context of composite Higgs models for the electroweak symmetry breaking. On the phenomenological side, scenarios involving momentum-dependent couplings can reproduce the observed dark matter abundance in the Universe, while evading the stringent bounds from direct detection experiments.

Monojet searches at the LHC are important probes of dark matter. In the context of a simplified model where a pair of dark matter particles η interacts with the Standard Model via a scalar mediator s, we considered two types of dark matter-mediator couplings, momentum-dependent or momentum-independent, corresponding to two operators with different Lorentz structures. The high-energy tail of the monojet differential distribution being harder in the momentum-dependent case, the associated cross-section is expected to be more efficiently constrained by current LHC data. We demonstrated this by studying the monojet cross section upper limits in the two scenarios, employing early 13 TeV LHC data. We showed that, indeed, one can probe smaller cross sections in the momentum-dependent case. The difference in sensitivity appears when the mediator is produced off-shell, $m_\eta > m_s/2$, and provided enough phase space is available, $m_\eta \lesssim 1$ TeV. This difference ranges from a factor of order one, for $m_\eta \sim m_s \sim 500$ GeV, up to one order of magnitude for lower masses, $m_\eta \sim m_s \sim 50$ GeV. We moreover estimated the reach of the LHC assuming an integrated luminosity of 300 fb^{-1} in proton-proton collisions at a center-of-mass energy of 13 TeV.

In the momentum-dependent case, that is free from direct detection constraints, we compared the monojet upper bounds on the dark matter couplings with the requirement of not exceeding the observed dark matter abundance in the Universe. While the present bounds correspond to under-abundant relic densities, the projected 300 fb^{-1} bounds become sensitive to the observed dark matter relic density for sufficiently light masses, $m_\eta, m_s \lesssim 100$ GeV. We also carefully checked that, in the relevant parameter space of

the model, our description in terms of effective operators is consistent with perturbative unitarity.

Our study indicates that, in the near future, the LHC can cover the most significant portion of the parameter space in the case of a light, off-shell mediator to the dark sector. Indeed, one can progressively close the gap between the collider upper limits on the dark matter couplings, and their values preferred by cosmological observations, assuming a standard thermal history. Were a monojet signal observed, the differences in the monojet p_T distribution between the momentum-dependent and the momentum-independent couplings could provide handles on the nature of the dark matter interactions with the Standard Model. One should keep in mind that, contrary to our simplifying assumption, both types of coupling can be present, but it is likely that one provides the dominant contribution. A discrimination among the two scenarios appears feasible, once the statistics become sufficient to analyse the shape of the distributions.

5 Acknowledgements

The authors are grateful to F. Maltoni for discussions about the unitarity constraints and to S. Lacroix for his fruitful participation to the early stage of this project. We would also like to thank the organizers of the 2015 'Les Houches – Physics at TeV colliders' workshop where this work was initiated.

MF has been partly supported by the OCEVU Labex (ANR-11-LABX-0060) and the A*MIDEX project (ANR-11-IDEX-0001-02) and by the European Union's Horizon 2020 research and innovation programme under the Marie Sködowska-Curie grant agreements No 690575 and No 674896. BF has been supported by the Theorie LHC France initiative of the CNRS, SK by the New Frontiers program of the Austrian Academy of Sciences, DS by the French ANR project DMAstroLHC (ANR-12-BS05-0006).

A Derivation of perturbative unitarity constraints

We follow the analysis presented in Ref. [38], using conventions essentially coinciding with those used by Jacob and Wick in their seminal paper on the computation of scattering amplitudes in terms of helicity eigenstates [57, 58]. In order to compute the range of validity of our effective field theory framework, we rely on the optical theorem,

$$\mathcal{M}_{i\to f} - \mathcal{M}^{\dagger}_{f\to i} = -i \sum_X \int \mathrm{d}\Pi^X_{\mathrm{LIPS}}\ (2\pi)^4 \delta^4(p_i - p_X)\ \mathcal{M}_{i\to X}\mathcal{M}^{\dagger}_{X\to f}\ , \tag{A.1}$$

where X represents a complete set of intermediate states in the amplitudes $\mathcal{M}$ and $\mathrm{d}\Pi^X_{\mathrm{LIPS}}$ the associated Lorentz-invariant phase space measure. This relation is exact and would hold if we could compute the amplitudes non-perturbatively, and should also hold order-by-order in perturbation theory. The case of interest to us is the one where $f \equiv i$, which gives

$$2\mathrm{Im}\left[\mathcal{M}_{i\to i}\right] = -i \sum_X \int \mathrm{d}\Pi^X_{\mathrm{LIPS}}\ (2\pi)^4 \delta^4(p_i - p_X)\ \left|\mathcal{M}_{i\to X}\right|^2\ . \tag{A.2}$$

For $2 \to 2$ reactions and adopting the center-of-momentum reference frame, all kinematic variables can be integrated over, except the angle θ between the collision axis and one of the final-state particle momenta,

$$2\mathrm{Im}\left[\mathcal{M}_{i\to i}\right] = \sum_f \beta_f \int \frac{\mathrm{d}\cos\theta}{16\pi} \left|\mathcal{M}_{i\to f}\right|^2 \ , \tag{A.3}$$

where β_f reads

$$\beta_f = \frac{\sqrt{[s-(m_1+m_2)^2]\,[s-(m_1-m_2)^2]}}{s} \ , \tag{A.4}$$

with $\sqrt{s}$ being the center-of-mass energy and m_1 and m_2 the masses of the outgoing particles.

The scattering amplitudes $\mathcal{M}_{i\to f}$ can be expanded in partial waves as

$$\mathcal{M}_{i\to f}(s,\cos\theta) = 8\pi \sum_{j=0}^{\infty} (2j+1) T^j_{i\to f}(s)\ d^j_{\lambda_f\lambda_i}(\theta) \ , \tag{A.5}$$

where j is the total angular momentum of the final state (2-body) system, λ_i and λ_f are the initial and final-state (2-body system) helicities, $T^j_{i\to f}(s)$ are the amplitudes describing the transition between the (definite helicity) states i and f for a given value of j and d are the Wigner d–functions. Multiplying both sides of the equation by $d^{j'}_{\lambda_f\lambda_i}(\theta)$, integrating over $\cos\theta$ from -1 to 1 and using the identity

$$\int_{-1}^{1} \mathrm{d}\cos\theta\ d^j_{\lambda_f\lambda_i}(\theta) d^{j'}_{\lambda_f\lambda_i}(\theta) = \frac{2}{2j+1}\delta_{j'j} \ , \tag{A.6}$$

the j-th partial wave amplitude between the definite helicity states λ_i and λ_f is given by

$$T^j_{i\to f}(s) = \frac{1}{16\pi} \int_{-1}^{1} \mathrm{d}\cos\theta \mathcal{M}_{i\to f}(s,\cos\theta) d^j_{\lambda_f\lambda_i}(\theta) \ . \tag{A.7}$$

One therefore obtains,

$$\mathrm{Im}(T^j_{i\to i}) = \sum_f \beta_f |T^j_{i\to f}|^2 = \beta_i |T^j_{i\to i}|^2 + \sum_{f\neq i} \beta_f |T^j_{i\to f}|^2 \ , \tag{A.8}$$

which yields the following restrictions for the transition amplitudes $T^j_{i\to f}(s)$,

$$\beta_i \mathrm{Re}\left[T^j_{i\to i}(s)\right] \leq 1 \ , \qquad \beta_i \mathrm{Im}\left[T^j_{i\to i}(s)\right] \leq 2 \ , \qquad \sum_{f\neq i} \beta_i\beta_f \left|T^j_{i\to f}(s)\right|^2 \leq 1 \ . \tag{A.9}$$

In order to compute the helicity amplitudes, we need explicit forms for the wave-functions of the external particles. We work in the Dirac representation throughout our calculation. Spinors of definite helicity $\lambda = \pm 1/2$, propagating in the direction (θ,ϕ) and describing particles with mass m and energy E are represented as

$$u(E,\theta,\phi,\lambda) = \begin{pmatrix} \sqrt{E+m}\ \chi_\lambda(\theta,\phi) \\ 2\lambda\sqrt{E-m}\ \chi_\lambda(\theta,\phi) \end{pmatrix} \quad \text{and} \quad v(E,\theta,\phi,\lambda) = \begin{pmatrix} \sqrt{E-m}\ \chi_{-\lambda}(\theta,\phi) \\ -2\lambda\sqrt{E+m}\ \chi_{-\lambda}(\theta,\phi) \end{pmatrix} \ , \tag{A.10}$$

where the Weyl spinors χ are given by

$$\chi_{1/2}(\theta,\phi) = \begin{pmatrix} \cos\frac{\theta}{2} \\ e^{i\phi}\sin\frac{\theta}{2} \end{pmatrix} \qquad \text{and} \qquad \chi_{-1/2}(\theta,\phi) = \begin{pmatrix} -e^{-i\phi}\sin\frac{\theta}{2} \\ \cos\frac{\theta}{2} \end{pmatrix} \ . \tag{A.11}$$

The conjugate spinors can be computed as usual with $\bar{u} = u^\dagger\gamma^0$ and similarly for $\bar{v}$, with γ^0 being taken in the Dirac representation. Polarisation vectors of massless vector fields are represented as

$$\epsilon^\mu_\pm = \frac{1}{\sqrt{2}} e^{\pm i\phi}\left(0, \mp\cos\theta\cos\phi + i\sin\phi, \mp\cos\theta\sin\phi - i\cos\phi, \pm\sin\theta\right) \ , \tag{A.12}$$

and four-momenta are finally written as

$$p = (p, p\sin\theta\cos\phi, p\sin\theta\sin\phi, p\cos\theta) \ . \tag{A.13}$$

The initial and final state helicities λ_i and λ_f appearing in Eq. (A.7) are defined as $\lambda_i = \lambda_1 - \lambda_2$ and $\lambda_f = \lambda_3 - \lambda_4$, as we consider a $2 \to 2$ collision where the colliding particles are labelled as 1, 2, 3 and 4. By convention, the particles 1 and 3 are chosen to propagate in the $(\theta,\phi) = (0,0)$ and $(\theta_f, 0)$ direction respectively, the choice $\phi = 0$ not affecting the results since all distributions of final-state particles are azimuthally symmetric. Consequently, the particles 2 and 4 propagate in the $(\pi-\theta, \pi+\phi) = (\pi,\pi)$ and $(\pi-\theta_f,\pi)$ direction respectively.

For the new physics model considered in this paper, we treat the momentum-dependent and momentum-independent operators separately. Extracting the Feynman rules from the momentum-independent part of the Lagrangian in Eq. (2.1), the transition amplitude for the $gg \to \eta\eta$ process reads

$$\mathcal{M}_{\rm MI} = \frac{\alpha_s c_{s\eta} c_{sg}}{4\pi} \epsilon_1^\mu \left(p_1^\mu p_2^\nu - g^{\mu\nu}(p_1\cdot p_2)\right)\epsilon_2^\nu \frac{1}{k^2 - m_s^2} \ . \tag{A.14}$$

The only non-zero partial amplitudes are associated with the transition $(+,+) \to (0,0)$,

$$T^0_{(+,+)\to(0,0)} = \frac{c_{sg}c_{s\eta}\alpha_s s}{64\pi^2(m_s^2 - s)} \ , \tag{A.15}$$

and similarly for $+ \leftrightarrow -$. Using the inequalities of Eq. (A.9), we get the following bound on $\kappa_{\rm MI} = c_{s\eta} \times c_{sg}$,

$$\kappa_{MI} < \frac{64\sqrt{2}\pi^2(1 - \frac{m_s^2}{s})}{\alpha_s\left(1 - \frac{4m_\eta^2}{s}\right)^{1/4}} \ , \tag{A.16}$$

where an extra factor of $1/2$ has been added to account for the identical final-state particles. For the momentum-dependent part of the Lagrangian, the transition amplitude reads

$$\mathcal{M}_{\rm MD} = \frac{\alpha_s c_{s\eta} c_{sg}}{4\pi} \epsilon_1^\mu \left(p_1^\mu p_2^\nu - g^{\mu\nu}(p_1\cdot p_2)\right)\epsilon_2^\nu \frac{k^2}{k^2 - m_s^2} \ . \tag{A.17}$$

Again, the only non-zero partial amplitudes are related to the transition $(+,+) \to (0,0)$,

$$T^0_{(+,+)\to(0,0)} = \frac{c_{sg}c_{\partial s\eta}\alpha_s s^2}{64\pi^2 f^2(m_s^2 - s)} \ , \tag{A.18}$$

and similarly for $+ \leftrightarrow -$. We then extract a bound on $\kappa_{\rm MD} = c_{\partial s\eta} \times c_{sg}$,

$$\kappa_{MD} < \frac{64\sqrt{2}\pi^2 f^2 (s - m_s^2)}{\alpha_s s^2 \left(1 - \frac{4m_\eta^2}{s}\right)^{1/4}} \ . \tag{A.19}$$

Focusing on the process $gg \to \eta\eta$, and for given values of masses and couplings, these relations can be used to extract the maximal allowed value for s for which our effective description makes sense perturbatively. Conversely, for a given value of s it can be used in order to bound the parameters of our model, see Section 3.3.

References

[1] **ATLAS** Collaboration, G. Aad et al., *Search for pair-produced third-generation squarks decaying via charm quarks or in compressed supersymmetric scenarios in pp collisions at $\sqrt{s} = 8$ TeV with the ATLAS detector*, *Phys. Rev.* **D90** (2014), no. 5 052008, [arXiv:1407.0608].

[2] **ATLAS** Collaboration, G. Aad et al., *Search for new phenomena in final states with an energetic jet and large missing transverse momentum in pp collisions at $\sqrt{s}$ =8 TeV with the ATLAS detector*, *Eur. Phys. J.* **C75** (2015), no. 7 299, [arXiv:1502.01518]. [Erratum: Eur. Phys. J.C75,no.9,408(2015)].

[3] **ATLAS** Collaboration, M. Aaboud et al., *Search for new phenomena in final states with an energetic jet and large missing transverse momentum in pp collisions at $\sqrt{s} = 13$ TeV using the ATLAS detector*, arXiv:1604.07773.

[4] **CMS** Collaboration, V. Khachatryan et al., *Search for dark matter, extra dimensions, and unparticles in monojet events in proton-proton collisions at $\sqrt{s} = 8$ TeV*, *Eur. Phys. J.* **C75** (2015), no. 5 235, [arXiv:1408.3583].

[5] **CMS** Collaboration, V. Khachatryan et al., *Searches for third-generation squark production in fully hadronic final states in proton-proton collisions at $\sqrt{s} = 8$ TeV*, *JHEP* **06** (2015) 116, [arXiv:1503.08037].

[6] T. G. Rizzo, *Identification of the Origin of Monojet Signatures at the LHC*, *Phys. Lett.* **B665** (2008) 361–368, [arXiv:0805.0281].

[7] O. Buchmueller, M. J. Dolan, S. A. Malik, and C. McCabe, *Characterising dark matter searches at colliders and direct detection experiments: Vector mediators*, *JHEP* **01** (2015) 037, [arXiv:1407.8257].

[8] G. Brooijmans et al., *Les Houches 2015: Physics at TeV colliders - new physics working group report*, in *9th Les Houches Workshop on Physics at TeV Colliders (PhysTeV 2015) Les Houches, France, June 1-19, 2015*, 2016. arXiv:1605.02684.

[9] M. Frigerio, A. Pomarol, F. Riva, and A. Urbano, *Composite Scalar Dark Matter*, *JHEP* **07** (2012) 015, [arXiv:1204.2808].

[10] D. Marzocca and A. Urbano, *Composite Dark Matter and LHC Interplay*, *JHEP* **07** (2014) 107, [arXiv:1404.7419].

[11] N. Fonseca, R. Z. Funchal, A. Lessa, and L. Lopez-Honorez, *Dark Matter Constraints on Composite Higgs Models*, *JHEP* **06** (2015) 154, [arXiv:1501.05957].

[12] I. Brivio, M. B. Gavela, L. Merlo, K. Mimasu, J. M. No, R. del Rey, and V. Sanz, *Non-linear Higgs portal to Dark Matter*, arXiv:1511.01099.

[13] S. Bruggisser, F. Riva, and A. Urbano, *The Last Gasp of Dark Matter Effective Theory*, arXiv:1607.02475.

[14] S. Bruggisser, F. Riva, and A. Urbano, *Strongly Interacting Light Dark Matter*, arXiv:1607.02474.

[15] **ATLAS** Collaboration, G. Aad et al., *Constraints on new phenomena via Higgs boson couplings and invisible decays with the ATLAS detector*, *JHEP* **11** (2015) 206, [arXiv:1509.00672].

[16] **CMS** Collaboration, V. Khachatryan et al., *Search for exotic decays of a Higgs boson into undetectable particles and one or more photons*, *Phys. Lett.* **B753** (2016) 363–388, [arXiv:1507.00359].

[17] **CMS** Collaboration, V. Khachatryan et al., *Precise determination of the mass of the Higgs boson and tests of compatibility of its couplings with the standard model predictions using proton collisions at 7 and 8 TeV*, *Eur. Phys. J.* **C75** (2015), no. 5 212, [arXiv:1412.8662].

[18] S. Lacroix, *Phénoménologie dun candidat de matière noire couplé au boson de Higgs*, *https://phystev.cnrs.fr/wiki/_media/2015:groups:higgs:dmhiggs:rapport.pdf*.

[19] N. Craig, H. K. Lou, M. McCullough, and A. Thalapillil, *The Higgs Portal Above Threshold*, arXiv:1412.0258.

[20] G. Panico and A. Wulzer, *The Composite Nambu-Goldstone Higgs*, *Lect. Notes Phys.* **913** (2016) pp.1–316, [arXiv:1506.01961].

[21] J. Alwall, C. Duhr, B. Fuks, O. Mattelaer, D. G. Öztürk, and C.-H. Shen, *Computing decay rates for new physics theories with FeynRules and MadGraph 5_aMC@NLO*, *Comput. Phys. Commun.* **197** (2015) 312–323, [arXiv:1402.1178].

[22] A. Alloul, N. D. Christensen, C. Degrande, C. Duhr, and B. Fuks, *FeynRules 2.0 - A complete toolbox for tree-level phenomenology*, *Comput. Phys. Commun.* **185** (2014) 2250–2300, [arXiv:1310.1921].

[23] **UA2** Collaboration, J. Alitti et al., *A Search for new intermediate vector mesons and excited quarks decaying to two jets at the CERN $\bar{p}p$ collider*, *Nucl. Phys.* **B400** (1993) 3–24.

[24] **CDF** Collaboration, T. Aaltonen et al., *Search for new particles decaying into dijets in proton-antiproton collisions at s**(1/2) = 1.96-TeV*, *Phys. Rev.* **D79** (2009) 112002, [arXiv:0812.4036].

[25] **CMS** Collaboration, V. Khachatryan et al., *Search for resonances and quantum black holes using dijet mass spectra in proton-proton collisions at $\sqrt{s} = 8$ TeV*, *Phys. Rev.* **D91** (2015), no. 5 052009, [arXiv:1501.04198].

[26] **ATLAS** Collaboration, G. Aad et al., *Search for new phenomena in the dijet mass distribution using $p-p$ collision data at $\sqrt{s} = 8$ TeV with the ATLAS detector*, *Phys. Rev.* **D91** (2015), no. 5 052007, [arXiv:1407.1376].

[27] G. Belanger, F. Boudjema, A. Pukhov, and A. Semenov, *Dark matter direct detection rate in a generic model with micrOMEGAs 2.2*, *Comput. Phys. Commun.* **180** (2009) 747–767, [arXiv:0803.2360].

[28] **Planck** Collaboration, P. A. R. Ade et al., *Planck 2015 results. XIII. Cosmological parameters*, arXiv:1502.01589.

[29] J. L. Feng, S. Su, and F. Takayama, *Lower limit on dark matter production at the large hadron collider*, *Phys. Rev. Lett.* **96** (2006) 151802, [hep-ph/0503117].

[30] G. Busoni, A. De Simone, T. Jacques, E. Morgante, and A. Riotto, *Making the Most of the Relic Density for Dark Matter Searches at the LHC 14 TeV Run*, *JCAP* **1503** (2015) 022, [arXiv:1410.7409].

[31] J. Hisano, K. Ishiwata, and N. Nagata, *Gluon contribution to the dark matter direct detection*, *Phys. Rev.* **D82** (2010) 115007, [arXiv:1007.2601].

[32] X. Chu, T. Hambye, T. Scarna, and M. H. G. Tytgat, *What if Dark Matter Gamma-Ray Lines come with Gluon Lines?*, *Phys. Rev.* **D86** (2012) 083521, [arXiv:1206.2279].

[33] M. A. Shifman, A. I. Vainshtein, and V. I. Zakharov, *Remarks on Higgs Boson Interactions with Nucleons*, *Phys. Lett.* **B78** (1978) 443.

[34] G. Bélanger, F. Boudjema, A. Pukhov, and A. Semenov, *micrOMEGAs4.1: two dark matter candidates*, *Comput. Phys. Commun.* **192** (2015) 322–329, [arXiv:1407.6129].

[35] **LUX** Collaboration, D. S. Akerib et al., *Improved WIMP scattering limits from the LUX experiment*, arXiv:1512.03506.

[36] **LUX** Collaboration, D. S. Akerib et al., *Results from a search for dark matter in LUX with 332 live days of exposure*, arXiv:1608.07648.

[37] I. M. Shoemaker and L. Vecchi, *Unitarity and Monojet Bounds on Models for DAMA, CoGeNT, and CRESST-II*, *Phys. Rev.* **D86** (2012) 015023, [arXiv:1112.5457].

[38] M. Endo and Y. Yamamoto, *Unitarity Bounds on Dark Matter Effective Interactions at LHC*, *JHEP* **06** (2014) 126, [arXiv:1403.6610].

[39] F. Kahlhoefer, K. Schmidt-Hoberg, T. Schwetz, and S. Vogl, *Implications of unitarity and gauge invariance for simplified dark matter models*, *JHEP* **02** (2016) 016, [arXiv:1510.02110].

[40] E. Conte, B. Fuks, and G. Serret, *MadAnalysis 5, A User-Friendly Framework for Collider Phenomenology*, *Comput. Phys. Commun.* **184** (2013) 222–256, [arXiv:1206.1599].

[41] E. Conte, B. Dumont, B. Fuks, and C. Wymant, *Designing and recasting LHC analyses with MadAnalysis 5*, *Eur. Phys. J.* **C74** (2014), no. 10 3103, [arXiv:1405.3982].

[42] D. Sengupta, *Madanalysis5 implementation of the ATLAS monojet and missing transverse momentum search documented in arXiv:1604.07773*, 10.7484/INSPIREHEP.DATA.GTH3.RN26.

[43] B. Dumont, B. Fuks, S. Kraml, S. Bein, G. Chalons, E. Conte, S. Kulkarni, D. Sengupta, and C. Wymant, *Toward a public analysis database for LHC new physics searches using MADANALYSIS 5*, *Eur. Phys. J.* **C75** (2015), no. 2 56, [arXiv:1407.3278].

[44] C. Degrande, C. Duhr, B. Fuks, D. Grellscheid, O. Mattelaer, and T. Reiter, *UFO - The Universal FeynRules Output*, *Comput. Phys. Commun.* **183** (2012) 1201–1214, [arXiv:1108.2040].

[45] J. Alwall, R. Frederix, S. Frixione, V. Hirschi, F. Maltoni, O. Mattelaer, H. S. Shao, T. Stelzer, P. Torrielli, and M. Zaro, *The automated computation of tree-level and*

next-to-leading order differential cross sections, and their matching to parton shower simulations, *JHEP* **07** (2014) 079, [arXiv:1405.0301].

[46] T. Sjöstrand, S. Mrenna, and P. Z. Skands, *PYTHIA 6.4 Physics and Manual*, *JHEP* **05** (2006) 026, [hep-ph/0603175].

[47] **DELPHES 3** Collaboration, J. de Favereau, C. Delaere, P. Demin, A. Giammanco, V. Lemaitre, A. Mertens, and M. Selvaggi, *DELPHES 3, A modular framework for fast simulation of a generic collider experiment*, *JHEP* **02** (2014) 057, [arXiv:1307.6346].

[48] M. Cacciari, G. P. Salam, and G. Soyez, *FastJet User Manual*, *Eur. Phys. J.* **C72** (2012) 1896, [arXiv:1111.6097].

[49] M. Cacciari, G. P. Salam, and G. Soyez, *The Anti-k(t) jet clustering algorithm*, *JHEP* **04** (2008) 063, [arXiv:0802.1189].

[50] A. L. Read, *Modified frequentist analysis of search results (The CL(s) method)*, in *Workshop on confidence limits, CERN, Geneva, Switzerland, 17-18 Jan 2000: Proceedings*, 2000.

[51] A. L. Read, *Presentation of search results: The CL(s) technique*, *J. Phys.* **G28** (2002) 2693–2704. [,11(2002)].

[52] T. Sjstrand, S. Ask, J. R. Christiansen, R. Corke, N. Desai, P. Ilten, S. Mrenna, S. Prestel, C. O. Rasmussen, and P. Z. Skands, *An Introduction to PYTHIA 8.2*, *Comput. Phys. Commun.* **191** (2015) 159–177, [arXiv:1410.3012].

[53] **ATLAS** Collaboration, *Expected Performance of the ATLAS Experiment - Detector, Trigger and Physics*, *SLAC-R-980, CERN-OPEN-2008-020* (2009) [arXiv:0901.0512].

[54] L. Moneta, K. Belasco, K. S. Cranmer, S. Kreiss, A. Lazzaro, D. Piparo, G. Schott, W. Verkerke, and M. Wolf, *The RooStats Project*, *PoS* **ACAT2010** (2010) 057, [arXiv:1009.1003].

[55] D. Abercrombie et al., *Dark Matter Benchmark Models for Early LHC Run-2 Searches: Report of the ATLAS/CMS Dark Matter Forum*, arXiv:1507.00966.

[56] C. Arina et al., *A comprehensive approach to dark matter studies: exploration of simplified top-philic models*, arXiv:1605.09242.

[57] M. Jacob and G. C. Wick, *On the general theory of collisions for particles with spin*, *Annals Phys.* **7** (1959) 404–428. [Annals Phys.281,774(2000)].

[58] H. E. Haber, *Spin formalism and applications to new physics searches*, in *Spin structure in high-energy processes: Proceedings, 21st SLAC Summer Institute on Particle Physics, 26 Jul - 6 Aug 1993, Stanford, CA*, 1994. hep-ph/9405376.